Elastic-Inelastic Buckling of Stiffened Panels Subject to Thermal Gradient

JOHN G. TAWRESEY* AND JAMES E. LIUM†
The Boeing Company, Seattle, Wash.

A solution for buckling of stiffened skins, riveted or integral, subject to thermal loads and stresses above the proportional limit is obtained by the use of small deflection energy methods. The effects of distortions of the stiffener and skin cross sections and the effects of thermal gradient are directly accounted for in the buckling determinant. Inelastic material behavior is analyzed by an iterative procedure. Early buckling of the skin between stiffeners is accounted for by a reduced modulus technique so that the ultimate panel loads are obtained from the determinant. The method has demonstrated good correlation with test data. An example calculation is presented.

Nomenclature

A_i = ith element area
b = spacing between stiffeners
C_{ij} = coefficient relating ϵ_i to κ_j
d_{ij} = coefficient relating u_i to ξ_j
E = elastic modulus
E_i = ith element tangent modulus
E_r = skin element reduced modulus
F_i = ith element thermal load
$f[X,Y]$ = coefficient relating the stiffener displacement to the skin-stiffener intersection rotation
G_i = ith element shear secant modulus
H_{ij} = coefficient relating δ_i to ξ_j
i = element index
I_i = moment of inertia ($l_i^3 t_i/12$)
I_i^o = moment of inertia/unit length ($t_i^3/12$)
I = identity matrix
j = mode index
J_i = ith element torsion constant ($l_i t_i^3/3$)
L = length between panel supports
l_i = ith element width
m = number of modes
n = number of elements
n_o = ratio of the panel critical strain to the skin critical strain
$\bar{P}$ = critical load
P = load on the ith element
$P_i S_k$ = kth skin element load
Q_j = coefficient of the assumed curvature functions, ξ_j
SX_{ij} = coefficient relating X_i to ξ_j
SY_{ij} = coefficient relating Y_i to ξ_j
$S\Theta_{ij}$ = coefficient relating Θ_i to ξ_j
t_i = ith element thickness
T_i = temperature of the ith element
u_i = ith element strain energy due to bending about the z_i axis
U_e = strain energy
U_p = work of the external loads
W_i = coefficients relating the element loads to the load, $\bar{P}$
(X,Y,Z) = general coordinate system
(x,y,z) = element coordinate system
X_i = ith element centroidal displacement in the X direction
Y_i = ith element centroidal displacement in the Y direction
α_i = coefficient of thermal expansion of the ith element
Δ_i = displacement of the ith element in the Z direction
δ_i = ith element displacement in the x_i direction
ϵ_i = ith element axial strain
Θ_i = ith element rotation
κ_i = ith element major principle axis curvature
ξ_j = assumed buckling curvature
σ = skin stress after skin buckling
Ω_t = total potential
$'$ = differentiation with respect to the Z axis
$\{\ \}$ = row vector
$[\ ]$ = rectangular matrix
$\overline{[\ ]}$ = diagonalized row matrix

Received April 12, 1971. Presented as Paper 71-338 at the AIAA/ASME 12th Structures, Structural Dynamics and Materials Conference, Anaheim, Calif., April 19–21, 1971; revision received September 27, 1971.

Index category: Structural Stability Analysis.

* Engineer, Structures Staff, Commercial Airplane Group. Member AIAA.

† Senior Specialist Engineer, Structures Staff, Commercial Airplane Group. Member AIAA.

I. Introduction

A METHOD for computing the critical end load of stiffened panels subject to a thermal environment is developed. Equations which account for thermal stresses, modulus changes due to temperature, stresses above the proportional limit and early skin buckling are developed by dividing the domain of the panel cross section into subdivisions and constructing energies for each portion in accordance with compatibility of the interior boundaries.

A basis for the development of the method was set forth by H. Bleich,[1] who generated the energy equations for evaluating the bending and twisting stability of thin-walled cross sections without relying upon Wagner's[2] concept of unit warping. In later studies, J. N. Goodier[3] identified and presented equations for the primary displacements and rotations of a stiffener connected to a sheet. However, correlation with test data was poor since distortions of the stiffener and sheet were omitted. Using the work previously presented by Goodier, J. H. Argyris[4] added linear springs to the panel idealization which absorbed energy in proportion to the primary displacements of the stiffener. In this way, Argyris approximated the distortion energies and obtained results which correlated well with test data. However, the method was limited to considerations of symmetric and antisymmetric modes and in addition could not be readily adapted to account for thermal gradients and inelastic material behavior.

The present method idealizes the panel similar to the Bleich idealization. Any number of skin or stiffner modes may be used depending on the required accuracy and the available resources. The panel is assumed simply supported at its ends and responds to a thermal gradient such that plane sections remain parallel. These boundary conditions approximate a panel which is supported by equally spaced rings or ribs typical of an airplane fuselage or wing. The total potential of the panel is obtained by classical energy methods. The minimum potential energy theorem is employed to obtain a buckling determinant of order equal to the number of modes selected.

Correlation with recent tests of titanium, *J*-section and *Z*-section stiffened panels is made. In support of the test program, the present method was used to obtain the most efficient distribution of material over the stiffener cross section. The resulting panel configurations demonstrated considerable increase in critical compression load over earlier configurations of equal weight. This paper presents the analytical method, a numerical example and the test to analysis correlation.

II. Development of the Equations

The equations to be developed are applicable to any open section stiffened panel which is simply supported at its ends and subject to thermal and axial loading. The stiffener and skin are divided into n thin, flat beam elements of length L, width l_i, and thickness t_i. The general coordinate system (X,Y,Z) is selected with the origin at the left skin boundary, the Y axis normal to the skin, and the Z axis parallel to the stiffener longitudinal axis. The compression loading is applied parallel to the Z axis. Each beam element geometry is assumed not to vary with Z and is oriented by a local coordinate system $(x,y,z)_i$ where x and y are the principal axes and z is parallel to the longitudinal axis. An example panel idealization is shown in Fig. 1.

The energy equations are developed as functions of assumed element curvatures in the X,Y plane, ξ_j. The number and type of curvatures selected depends on the panel being considered and the required accuracy. An example curvature set for the panel in Fig. 1 is shown in Fig. 2.

The assumed curvature must be selected to satisfy the appropriate boundary conditions. By expressing the panel displacements as functions of the assumed curvatures, sufficient constraints on the curvatures can be found. The skin displacement in the Y direction may be written as an integral of the form

$$w_{sk} = \sum_j \iint \xi_j dX dX; \qquad j = \text{skin mode} \tag{1}$$

The stiffener displacements depend on the skin rotation and displacement at the stiffener skin intersection, and on the stiffener curvatures. The expression for the stiffener displacement takes the form:

$$w_{st} = \sum_k \iint \xi_k ds ds + \left\{\sum_j \int \xi_j dX\right\} \cdot f[X,Y] + \sum_j \iint \xi_j dX dX; \qquad k = \text{stiffener mode} \tag{2}$$

where s is a path in the X,Y plane. The simply supported boundary conditions at the panel ends require that:

$$w_{sk} = w_{st} = w_{sk}'' = w_{st}'' = 0; \qquad Z = 0, L \tag{3}$$

which is satisfied if:

$$\xi_j = \xi_j'' = 0; \qquad Z = 0, L \tag{4}$$

The boundary conditions at the panel edge depend on the assumed skin curvatures. Selection of sin functions in X may be used to satisfy simply supported edge conditions:

$$\int_0^{\text{edge}} \int \xi_j dX dX = 0 \quad \text{and} \quad \xi_j = 0; \qquad X = 0, \text{edge} \tag{5}$$

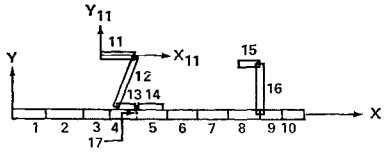

Fig. 1 Example panel idealization.

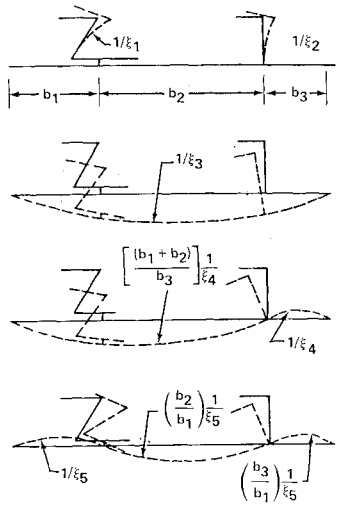

Fig. 2 Example buckling modes.

The boundary conditions for the piece-wise constant curvatures selected in Fig. 2 are:

$$\int_0^{\text{edge}} \int \xi_j dX dX = 0 \quad \text{and} \quad d\xi_j/dX = 0; \qquad X = 0, \text{edge} \tag{6}$$

For thin skins and wide panels, the critical load will not be sensitive to the unloaded edge boundary conditions. In formulating the equations which follow, constant curvatures for each element and the resulting boundary conditions of Eq. (6) are assumed.

Applying the Kirchhoff-Love assumption that plane sections remain plane to each beam element, the strain energy of the panel can be expressed as the sum of the beam element strain energies:

$$U_e = \frac{1}{2} \sum_{i=1}^{n} \int_0^L \{E_i I_i \kappa_i^2 + E_i A_i \epsilon_i^2 + G_i J_i \Theta_i'^2\} dZ + \sum_{i=1}^{n} u_i \tag{7}$$

where κ_i is the curvature due to bending about an axis which passes through the element centroid and is parallel to the y_i axis. ϵ_i is the strain at the element centroid and Θ_i is the element rotation. The quantity u_i is the strain energy for the ith element due to bending about the z_i axis:

$$u_i = \frac{1}{2} \int_0^L E_i I_i^o \left[\int_0^{l_i} \left(\sum_{j=1}^{m} d_{ij} \xi_j \right)^2 dx_i \right] dZ \tag{8}$$

where $d_{ij} = 1$ if the jth mode results in z_i axis bending of the ith element, otherwise $d_{ij} = 0$. Since ξ_j is assumed constant in x_i, u_i becomes:

$$u_i = \frac{1}{2} \int_0^L E_i I_i^o l_i \left(\sum_{j=1}^{m} d_{ij} \xi_j \right)^2 dZ \tag{9}$$

The bending curvatures κ_i are expressed as functions of the assumed modes by defining H_{ij} coefficients which satisfy:

$$\delta_i = \sum_{j=1}^{m} H_{ij} \xi_j \tag{10}$$

and differentiating with respect to Z,

$$\kappa_i = \sum_{j=1}^{m} H_{ij} \xi_j'' \tag{11}$$

The element rotations are related to the assumed modes by defining $S\Theta_{ij}$ coefficients such that:

$$\Theta_i = \sum_{j=1}^{m} S\Theta_{ij} \xi_j \tag{12}$$

The compatibility of axial strains between elements is used to define the relationship between the element curvatures κ_i and the axial strains ϵ_i. One compatibility equation can be written at each of the element intersections forming $n-1$ equations of the form:

$$\epsilon_i + \kappa_i l_i/2 = \epsilon_{i+1} + \kappa_{i+1} l_{i+1}/2 \tag{13}$$

An additional equation is obtained by assuming that the end load remains constant during buckling:

$$\sum_{i=1}^{n} E_i A_i \epsilon_i = 0 \tag{14}$$

Combining Eqs. (13) and (14) to form n equations for the n strains ϵ_i and solving:

$$\epsilon_i = \sum_{k=1}^{n} C_{ik} \kappa_k \tag{15}$$

Using Eqs. (7,9,11,12 and 15), the strain energy becomes:

$$U_e = \frac{1}{2}\int_0^L \sum_{i=1}^{n} \left\{ E_i I_i \left[\sum_{j=1}^{m} H_{ij} \xi_j'' \right]^2 + E_i A_i \left[\sum_{k=1}^{n} C_{ik} \left(\sum_{j=1}^{m} H_{kj} \xi_j'' \right) \right]^2 + G_i J_i \left[\sum_{j=1}^{m} S\Theta_{ij} \xi_j' \right]^2 + E_i I_i^o l_i \left[\sum_{j=1}^{m} d_{ij} \xi_j \right]^2 \right\} dZ \tag{16}$$

The work of the external loads is obtained by summing the work done on each element due to the displacements caused by the ξ_j curvatures:

$$U_p = -\sum_{i=1}^{n} P_i \Delta_i \tag{17}$$

The load P_i is the sum of the external applied load and the thermal load. Assuming that the panel is free to expand longitudinally when subjected to thermal loading, P_i is written as:

$$P_i = \left\{ E_i A_i \bar{P} / \sum_{k=1}^{n} E_k A_k \right\} + E_i A_i \left\{ -\alpha_i T_i + \left(\sum_{k=1}^{n} E_k A_k \alpha_k T_k \right) \Big/ \left(\sum_{k=1}^{n} E_k A_k \right) \right\} \tag{18}$$

where $\bar{P}$ is the critical end load. Equation (18) is expressed for convenience as:

$$P_i = \bar{P} W_i + F_i \tag{19}$$

The displacements Δ_i are obtained from:

$$\Delta_i = \frac{1}{2}\int_0^L [X_i'^2 + Y_i'^2 + (l_i^2/12) \cdot \Theta_i'^2] dZ \tag{20}$$

where X_i and Y_i are the displacements of the element centroids and may be written as linear functions of the ξ_j modes by defining SX_{ij} and SY_{ij} coefficients which satisfy:

$$X_i = \sum_{j=1}^{m} SX_{ij} \xi_j \tag{21}$$

$$Y_i = \sum_{j=1}^{m} SY_{ij} \xi_j \tag{22}$$

Applying Eqs. (12,21 and 22), and substituting Eqs. (20) and (19) into Eq. (17), the work of the external loads becomes:

$$U_p = -\frac{1}{2}\int_0^L \sum_{i=1}^{n} \left\{ (\bar{P} W_i + F_i) \left(\left[\sum_{j=1}^{m} SX_{ij} \xi_j' \right]^2 + \left[\sum_{j=1}^{m} SY_{ij} \xi_j' \right]^2 + \left[\sum_{j=1}^{m} S\Theta_{ij} \xi_j' \right]^2 \frac{l_i^2}{12} \right) \right\} dZ \tag{23}$$

The total potential is the sum of Eqs. (23) and (16):

$$\Omega_t = U_e + U_p \tag{24}$$

The modes ξ_j must be selected to satisfy the boundary conditions of Eq. (4). Since the edge boundary conditions have already been established, the following form for ξ_j satisfies all specified boundary conditions:

$$\xi_j = Q_j \sin \bar{n} Z \tag{25}$$

where Q_j is a constant in Z, $\bar{n} = N\pi/L$ and N is the wave number. Substituting Eq. (25) into Eq. (24), minimizing with respect to the coefficients Q_j and performing the integration, the following set of linear homogeneous equations is obtained:

$$0 = \partial\Omega_t/\partial Q_s = \frac{L}{4} \sum_{q=1}^{m} \left\{ \sum_{i=1}^{n} \left[E_i I_i H_{iq} H_{is} \bar{n}^4 + E_i A_i \left(\sum_{k=1}^{n} C_{ik} H_{kq} \right) \left(\sum_{k=1}^{n} C_{ik} H_{ks} \right) \bar{n}^4 + G_i J_i S\Theta_{iq} S\Theta_{is} \bar{n}^2 + E_i I_i^o l_i d_{iq} d_{is} - (\bar{P} W_i + F_i)(SX_{iq} SX_{is} + SY_{iq} SY_{is} + (l_i^2/12) S\Theta_{iq} S\Theta_{is}) \bar{n}^2 \right] \right\} Q_q; \qquad s = 1, m \tag{26}$$

This set of homogeneous equations can be written as:

$$[B - \bar{P} D][Q] = 0 \tag{27}$$

or

$$[D^{-1} B - \bar{P} I][Q] = 0 \tag{28}$$

where the B matrix contains stiffness and thermal load terms and the D matrix contains external work terms. The equations have a nontrivial solution if, and only if, the determinant of the coefficients is zero:

$$\det[D^{-1} B - \bar{P} I] = 0 \tag{29}$$

The critical load is the minimum value of $\bar{P}$ which satisfies Eq. (29).

The buckling determinant was constructed to accommodate different material properties for each element. Except for the thermal stress influence on Eq. (18), it is by means of E_t and G_t that the effects of plasticity, temperature distribution and skin buckling are incorporated into the analysis. The material modulus dependence on the total stress (thermal stress plus end load stress) and on temperature is found by linearly interpolating between Ramberg-Osgood material idealizations formulated at different temperatures. The influence of early skin buckling is accounted for by reducing skin element moduli. By applying Timoshenko's large deflection analysis of a plate loaded by a constant end strain to the skin between two stiffeners, the actual stress in the skin is found as a function of the panel axial strain:

$$\sigma = (Et^2/b^2)[6.96(n_o - 1)(\cos \pi x/b - .366) \times \cos \pi x/b - 4.25 n_o + .632] \tag{30}$$

where x is zero midway between the stiffeners, b is the skin bay width and t is the skin thickness. n_o is the ratio of the panel strain to the plate critical strain and is given as:

$$n_o = P_i b^2/(A_i E_i K_s t^2) \tag{31}$$

The subscript i designates a stiffener element and K_s is the plate buckling coefficient (the value selected for this study was 3.62). The load in the kth skin element is obtained by integrating Eq. (30) over the width of the kth element:

$$PS_k = \int_{l_k} t\sigma dx \tag{32}$$

Since this loading must result in a strain which is compatible with the stringer strain, the following relation for the reduced modulus is obtained:

$$E_r = A_i P S_k E_i/(A_k P_i) \tag{33}$$

This formulation assumes the load PS_k is uniformly distributed over the element. Thus, several skin elements must be used between stringers in order to approximate the distribution of Eq. (30). Unlike the effective width methods for skin buckling, this procedure approximates the actual load distribution as well as the load magnitude and therefore results in better values for the energies associated with the buckled skin.

An iterative procedure is required to obtain compatibility between stress, material properties, and skin buckling effects. The iteration technique recommended varies upper and lower bounds of each element stress until the critical end load converges to within set bounds. Initially, the upper bound is equal to the material yield stress, the lower bound is zero and the iteration stress, which is used to calculate new material properties for the next solution, is equal to the material proportional limit. On each successive iteration, the solution stress is used to set the variable upper and lower bounds. If the solution stress exceeds the iteration stress, the lower bound is set equal to the iteration stress. If the solution stress is less than the iteration stress, the upper bound is set equal to the iteration stress. The next iteration stress is selected as the average of the new upper and lower bound and the process continues until the desired accuracy is obtained. This method allows simultaneous iterations on the reduced skin moduli and the element material properties.

III. Example

The example is simplified to allow for hand or desk calculator computations. To do this the following points are observed. 1) The panel is assumed to be infinitely wide. The stiffener and skin geometry is shown in Fig. 3. 2) The material is assumed linearly elastic. 3) The skin between stiffeners is assumed not to buckle. 4) Four elements are used to idealize the section, Fig. 4. 5) Three modes are used as shown in Fig. 4. Mode 1 is a constant curvature extending from minus infinity to plus infinity and is equivalent to the classical flexural mode.

Matrix operations will be used in this example because they are convenient for the required hand calculations. The normal application of the method requires programing on a digital computer.

The panel geometry and material properties are:

$$\{E\} = \{14.8 \quad 15.5 \quad 16.4 \quad 16.4\} \times 10^6 \text{(psi)}$$
$$\{G\} = \{5.69 \quad 5.96 \quad 6.31 \quad 6.31\} \times 10^6 \text{(psi)}$$
$$\{t\} = \{.070 \quad .050 \quad .050 \quad .050\} \text{(in)}$$
$$\{l\} = \{1.00 \quad 2.00 \quad 3.00 \quad 3.00\} \text{(in)}$$

In addition the following values are required:

$$\{EI\} = \{0.0863 \quad 0.5167 \quad 1.8450 \quad 1.8450\} \times 10^6 \text{(lb-in}^2\text{)}$$
$$\{EI^o l\} = \{4.230 \quad 3.229 \quad 5.125 \quad 5.124\} \times 10^2 \text{(lb-in}^2\text{)}$$
$$\{EA\} = \{1.04 \quad 1.55 \quad 2.46 \quad 2.46\} \times 10^6 \text{(lb)}$$
$$\{GJ\} = \{6.50 \quad 4.96 \quad 7.89 \quad 7.89\} \times 10^2 \text{(lb-in}^2\text{)}$$
$$\bar{n} = 0.3491(1/\text{in}); \quad N = 1$$

The d_{ij} coefficients of Eq. (8) are inserted into a matrix such that the column index identifies the mode and the row index identifies the element:

$$[d] = \begin{bmatrix} 0 & 0 & 0 \\ 0 & 0 & 1 \\ 0 & 1 & 0 \\ 0 & 1 & 0 \end{bmatrix}$$

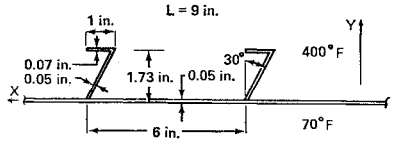

Fig. 3 Numerical example, panel geometry.

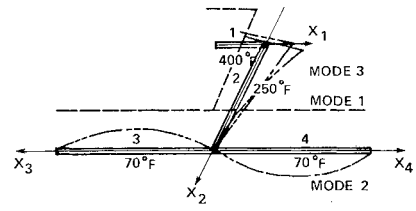

Fig. 4 Numerical example, panel idealization.

The H_{ij} and $S\Theta_{ij}$ coefficients of Eqs. (11) and (12) are constructed in the same manner:

$$[H] = \begin{bmatrix} 0 & 2.598 & 1.732 \\ -.866 & 0 & 0 \\ 0 & 0 & 0 \\ 0 & 0 & 0 \end{bmatrix} \text{(in}^2\text{)}$$

$$[S\Theta] = \begin{bmatrix} 0 & 1.5 & 2.0 \\ 0 & 1.5 & 0 \\ 0 & 0 & 0 \\ 0 & 0 & 0 \end{bmatrix} \text{(in)}$$

As an example calculation, consider element H_{13} of the above matrix. This quantity is the displacement of element 1 in the x_1 direction due to a unit curvature for mode 3, with all other modes constrained. Thus:

$$H_{13} = \left[\int_0^{l_2}\int_0^{l_2} dx_2 dx_2\right] \cos 30^\circ = 1.732 \text{ in}^2$$

The compatibility equations are constructed at each element intersection forming three equations.

$$\epsilon_1 + .5\kappa_1 = \epsilon_2 - \kappa_2, \quad \epsilon_2 + \kappa_2 = \epsilon_3 - 1.5\kappa_3,$$
$$\epsilon_2 + \kappa_2 = \epsilon_4 - 1.5\kappa_4$$

Applying Eq. (14), the following matrix equation is obtained:

$$\begin{bmatrix} 1. & -1. & 0 & 0 \\ 0 & 1. & -1. & 0 \\ 0 & 1. & 0 & -1. \\ 1.04 & 1.55 & 2.46 & 2.46 \end{bmatrix} \begin{bmatrix} \epsilon_1 \\ \epsilon_2 \\ \epsilon_3 \\ \epsilon_4 \end{bmatrix}$$
$$= \begin{bmatrix} -0.5 & -1. & 0 & 0 \\ 0 & -1. & -1.5 & 0 \\ 0 & -1. & 0 & -1.5 \\ 0 & 0 & 0 & 0 \end{bmatrix} \begin{bmatrix} \kappa_1 \\ \kappa_2 \\ \kappa_3 \\ \kappa_4 \end{bmatrix}$$

By inverting the left hand coefficient matrix and premultiplying the result times the right hand coefficient matrix, the C_{ij} coefficients of Eq. (15) are found:

$$[C] = \begin{bmatrix} -0.431 & -1.518 & -0.492 & -0.492 \\ 0.069 & -0.518 & -0.492 & -0.492 \\ 0.069 & 0.482 & 1.008 & -0.492 \\ 0.069 & 0.482 & -0.492 & 1.008 \end{bmatrix} \text{(in)}$$

The SX_{ij} and SY_{ij} coefficients are formulated in an analogous manner to the H_{ij} and $S\Theta_{ij}$ coefficients

$$[SX] = \begin{bmatrix} 0 & -2.598 & -1.732 \\ 0 & -1.299 & -0.744^* \\ 0 & 0^* & 0 \\ 0 & 0^* & 0 \end{bmatrix} \text{(in}^2\text{)}$$

$$[SY] = \begin{bmatrix} 1. & -0.75 & 1. - 1. = 0 \\ 1. & -0.75 & -0.447^* \\ 1. & 0.822^* & 0 \\ 1. & -0.822^* & 0 \end{bmatrix} \text{(in}^2\text{)}$$

The determination of element axial displacements for the external work calculations is better represented by considering variable displacements of the $d_{ij} \neq 0$ mode-element entries. Therefore, these SX and SY terms are calculated as follows. The external work is expressed as:

$$w_{ij} = P_i/A_i \int_0^{l_i} t_i \left(\frac{1}{2} \int_0^L \{\bar{\delta}_i'\}^2 dZ \right) dx_i \tag{34}$$

where the displacement $\bar{\delta}$ is a function of the element local coordinate x_i:

$$\bar{\delta}_i = \iint \xi_j dx_i dx_i \tag{35}$$

Using the following mode boundary conditions

$$\bar{\delta}_2 = d\bar{\delta}_2/dx_2 = 0; \quad @x_2 = l_2 \quad \bar{\delta}_i = 0, @x_i = 0, l_i; \quad i = 3,4 \tag{36}$$

Equation (36) is integrated to obtain:

$$\begin{aligned} \bar{\delta}_2 &= (x^2/2 - l_2 x + l_2^2/2)\xi_3 \\ \bar{\delta}_i &= \frac{1}{2}(x_i^2 - x_i l_i)\xi_i; \qquad i = 3,4 \end{aligned} \tag{37}$$

Substituting into the work equation and integrating, the work becomes:

$$\begin{aligned} w_{23} &= \frac{P_2}{2} \int_0^L (l_2^4/20)\xi_3'^2 dZ \\ w_{i2} &= \frac{P_i}{2} \int_0^L (l_i^4/120)\xi_2'^2 dZ; \qquad i = 2,3 \end{aligned} \tag{38}$$

By comparison with Eq. (23), it is concluded that the term within the parenthesis is the square of the desired displacement and is oriented in the local y_i direction. Taking components of this displacement in the X and Y directions results in the starred values of SX and SY. For example, SY_{23} is obtained from:

$$SY_{23} = \left(\frac{16}{20}\right)^{0.5} \sin 30^\circ = -.477 \text{ (in}^2\text{)}$$

Using Eq. (18), the W_i and F_i quantities are calculated:

$$\{W\} = \{0.1380 \quad 0.2065 \quad 0.3277 \quad 0.3277\}$$
$$\{F\} = \{1193.5 \quad 1010.6 \quad -1102.0 \quad -1102.0\} \text{ (lb)}$$

where the thermal expansions were taken as

$$\{\alpha T\} = \{0.0016 \quad 0.0011 \quad 0.0 \quad 0.0\} \text{ (in./in.)}$$

Finally, the B coefficients of Eq. (27) are found by performing the following matrix operations which are equivalent to the summations of Eq. (26).

$$\begin{aligned} [B] = {} & ([\overline{EI}][H])^T[H]\bar{n}^4 + ([\overline{EA}]([C][H]))^T([C][H])\bar{n}^4 + \\ & ([\overline{GJ}][S\Theta])^T[S\Theta]\bar{n}^2 + ([\overline{EI^o l}][d])^T[d] - \\ & ([\bar{F}][SX])^T[SX]\bar{n}^2 - ([\bar{F}][SY])^T[SY]\bar{n}^2 - \\ & ([\bar{F}][\overline{I^2/12}][S\Theta])^T[S\Theta]\bar{n}^2 \end{aligned}$$

$$= \begin{bmatrix} 4.969 & -2.605 & -1.745 \\ -2.605 & 3.108 & 2.006 \\ -1.745 & 2.006 & 1.384 \end{bmatrix} \times 10^4 \text{ (lb-in}^2\text{)}$$

where the row matrices are diagonalized. The D coefficients of Eq. (22) are calculated in a similar fashion:

$$[D] = \begin{bmatrix} 0.1218 & -0.0315 & -0.0112 \\ -0.0315 & 0.2556 & 0.1136 \\ -0.0112 & 0.1136 & 0.0762 \end{bmatrix} \text{ (in}^2\text{)}$$

By inverting D and premultiplying the result times the B matrix, the buckling determinant is found:

$$[\det] = \begin{bmatrix} 4.003 - \lambda & -1.945 & -1.317 \\ 0.6805 & -0.1979 - \lambda & -0.2932 \\ -2.714 & 2.641 & 2.060 - \lambda \end{bmatrix} \times 10^5 \text{ (lb)}$$

The three eigenvalues are:

$$\{\lambda\} = \{473277. \quad 90140. \quad 23136.\} \text{ (lb)}$$

from which the critical load of 23136. lb is found.

IV. Test to Analysis Correlation

All test panels were constructed of 6AL-4V Titanium alloy. The skins were continuously rolled, mill-annealed sheets. Three stiffener types were evaluated. These were draw-formed zee sections (1*A*, 1*B*, and 2*A*) of mill-annealed sheet, Fig. 5; machined, mill-annealed zee section extrusions (3*A*, 3*B*, 4*A*, and 5*A*) and machined, heat-treated *J*-section extrusions (6*A*, 6*B*, and 6*C*). Two panel sizes were tested, "single-bay" panels, with two simulated frames and four stiffeners and

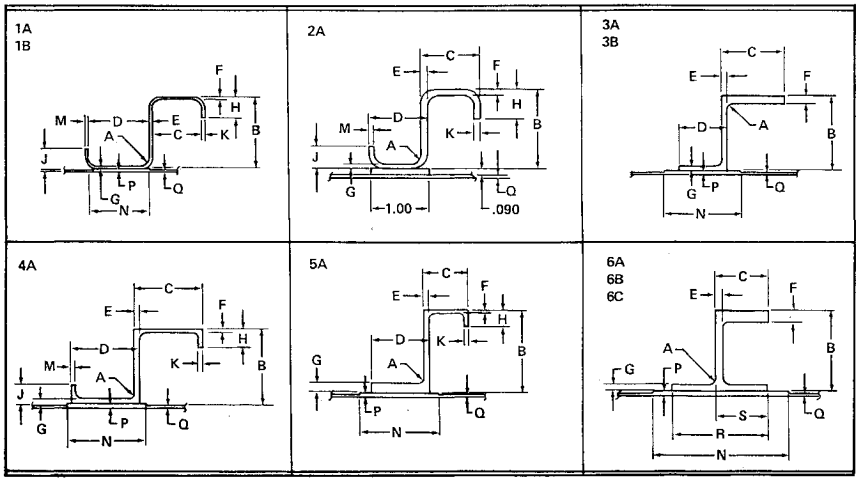

Fig. 5 Titanium test panels, skin and stiffener details.

Table 1 Titanium test panels, skin and stiffener geometries

STRINGER TYPE	DIMENSIONS																	
	A RAD	B	C	D	E	F	G	H	J	K	M	N	P	Q	R	S	L	b
1A	.15	1.25	.85	1.00	.040	.040	.040	.36	.36	.040	.040	1.00	.036	.030	–	–	17.75	4.5
1B	.15	1.25	.85	1.00	.050	.050	.050	.36	.36	.040	.040	–	–	.036	–	–	17.75	4.5
2A	.19	1.35	1.00	1.00	.090	.090	.090	.50	.40	.090	.090	–	–	.050	–	–	18.0	6.6
3A	.09	1.25	1.06	.85	.084	.120	.084	–	–	–	–	1.36	.056	.040	–	–	17.75	6.6
3B	.09	1.25	.50	.83	.070	.090	.100	–	–	–	–	1.36	.056	.040	–	–	17.75	6.6
4A	.09	1.25	1.14	1.14	.072	.072	.072	.33	.33	.072	.072	1.36	.056	.040	–	–	17.75	6.6
5A	.09	1.40	.715	.97	.070	.050	.145	.30	–	.045	–	1.36	.056	.040	–	–	17.75	6.6
6A	.09	1.58	1.04	–	.200	.300	.160	–	–	–	–	3.00	.071	.040	2.30	1.22	17.75	4.5
6B	.09	1.35	.90	–	.110	.180	.110	–	–	–	–	2.30	.071	.036	1.60	.85	17.75	4.5
6C	.09	1.40	.80	–	.075	.115	.100	–	–	–	–	2.30	.071	.050	1.60	.84	17.75	6.6

"multi-bay" panels with four simulated frames and six stiffeners. Nominal skin and stiffener dimensions for the panels are summarized in Table 1.

The test data correlation was based on actual detail dimensions and material properties for each panel. It is anticipated that this data will be published under a Department of Transportation contract. Application of the analysis used two web constant element curvatures, a flexural mode and a skin mode. The flexural mode and element curvatures were formulated as in the example. The skin mode was similar to the example, except the curvature was assumed to vary as the curvature of a cantilevered beam fixed at the stringer skin intersection and loaded by a concentrated force mid-bay between stringers. For later discussion, this skin mode will be referred to as the torsion mode. Table 2 presents the test and analytic load comparisons.

V. Discussion

The determinant of Eq. (29) is generally fully populated representing stiffness and load coupling between all assumed modes. Load coupling effects are shown in Fig. 6 for a 3*A* stiffener and skin. The coupling is primarily between symmetric torsion and flexure. The plot of stress level versus free flange width has two distinct regions, one of increasing stress and the other of decreasing stress. The stress increases in the first region because the increase in warping torsional stiffness exceeds the loss due to increased load coupling. As the flange width increases beyond 0.38 in., however, the loss due to load coupling dominates and the stress decreases. The over-all panel load continues to rise as L_2 increases since the area of the section is increasing.

Although this section is primarily governed by symmetric torsion and flexural modes, the reduction in critical load due to the web distortion curvatures varies between 15% for $L_2 = .45$ in. and 3.5% for $L_2 = 1.3$ in. From this it is evident that the inclusion of the stiffener modes is essential to obtain consistent correlations.

The present analysis was employed to study parameter variations on the sections in the hope of increasing panel efficiency. Due to limited available time and resources, the study was constrained to the four modes described above and to sections which resemble those originally sized. The trend evolved was to redistribute stiffener material such that the attached skin flange is significantly huskier than the outstanding flange. The 3*B* and 5*A* panel tests are examples. These sections demonstrated significant improvements in efficiency. Special note should be made that the structural efficiency of these sections was first determined analytically and subsequently verified by test.

Table 2 Test and analytic load comparison

Panel		Stiff-	Uniform	Thermal Gradient Temperature						Ratio
Single Bay	Multi-Bay	ener Type	Tempera-ture	Skin Mid-Bay	Skin Flange	Web	Free Flange	Test Load	Analysis Load	Test / Analysis
1A1S		1A	RT					40.2	40.8	.985
1A2S		1A	RT					41.7	41.0	1.017
1A3S		1A	-	50	110	320	410	34.6	31.7	1.092
1A4S		1A	-	430	370	215	120	35.5	43.3	.819
1B1S		1B	RT					52.8	56.4	.936
1B2S		1B	RT					53.7	55.5	.968
1B3S		1B	-	70	150	330	410	43.7	42.5	1.029
1B4S		1B	RT					57.4	56.6	1.015
1B5S		1B	450					51.8	50.8	1.020
	1B1M	1B	RT					69.4	77.9	.891
	1B2M	1B	RT					76.8	86.2	.891
2A1S		2A	RT					134.5	133.8	1.005
	2A1M	2A	RT					185.0	201.3	.919
3A1S		3A	RT					106.7	103.5	1.031
3A2S		3A	RT					122.0	109.1	1.118
3A3S		3A	-	60	130	325	410	96.2	84.0	1.145
3A4S		3A	RT					118.7	112.5	1.055
	3A1M	3A	-	60	130	325	410	152.0	137.9	1.102
	3A2M	3A	RT					155.0	174.8	.887
3B1S		3B	RT					96.7	98.9	.977
4A1S		4A	RT					111.4	115.1	.968
4A2S		4A	RT					106.0	116.4	.911
4A3S		4A	RT					104.7	114.2	.916
	4A1M	4A	RT					142.7	163.8	.871
5A1S		5A	RT					130.7	139.1	.939
6A1S		6A	RT					480.5	525.2	.915
6A2S		6A	RT					470.5	532.7	.883
6A3S		6A	-	65	225	320	385	420.5	449.1	.936
6A4S		6A	-	370	250	170	95	414.0	461.0	.898
6A5S		6A	450					388.0	399.0	.972
	6A1M	6A	RT					708.0	794.0	.891
6B1S		6B	RT					236.2	218.6	1.080
6B2S		6B	RT					237.0	228.0	1.039
6C1S		6C	RT					202.7	176.3	1.150
6C2S		6C	RT					178.2	167.3	1.065

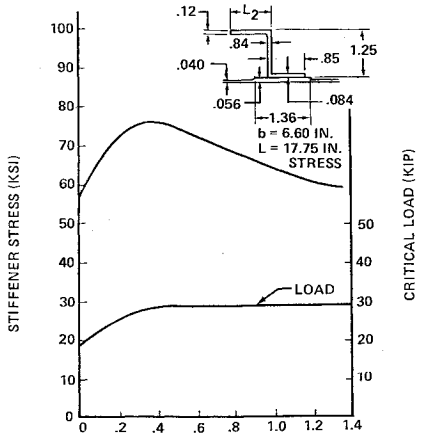

Fig. 6 Free flange length variation.

A stiffened skin panel, upon exposure to a thermal gradient, is assumed to expand such that plane sections remain parallel. This boundary condition implies that the sum of the element thermal loads is zero and therefore these loads do no external work for the classical flexure mode. The thermal loads, however, do influence the external work on the other modes. In addition, the strain energy is dependent on the changes in material moduli induced by temperature and thermal plus end load stress. Thus, the critical load exhibits a complex dependency on changes in load distribution and material properties, particularly when all or some element stresses exceed the proportional limit.

The results of an analysis performed on the 3A geometry are shown to illustrate the sensitivity of the method to varying temperature distributions and failure modes. Figures 7, 8 and 9 plot the relationships between thermal gradients, ultimate panel loads and stress distributions. Column lengths of 65 in., 17.75 in. and 7.0 in. were selected to vary the mode of failure from flexure-elastic to flexure-torsion-elastic to flexure-torsion-inelastic. The thermal gradient is defined as the difference between the free flange temperature and the skin temperature. Considering airframe supersonic heating, negative gradients are ascent thermal heating conditions and positive gradients are descent thermal heating conditions. The ratio of stress or load at the thermal gradient to the stress or load at a uniform 70°F temperature is given as the ordinate.

In Fig. 7, the flexure-elastic critical load decreases with increasing ascent or descent gradient due to temperature induced modulus reductions. Whereas thermal compression stresses are additive to the end load stress on hot elements, the free flange compression stress increases with increasing gradient. The skin flange stress decreases with increasing gradient because of thermally induced tension stresses.

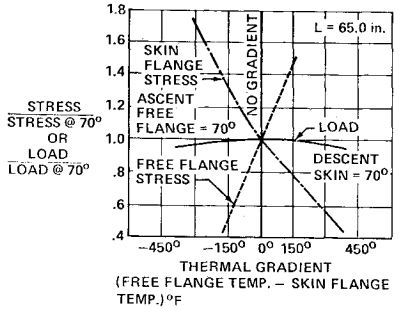

Fig. 7 Stress and load vs thermal gradient, flexure elastic section.

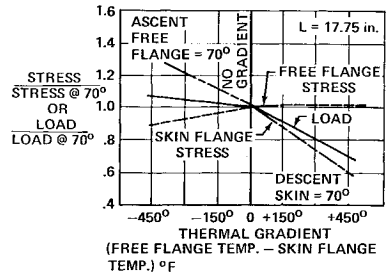

Fig. 8 Stress and load vs thermal gradient, flexure-torsion elastic section.

The thermal gradients affect the elastic and inelastic flexure-torsion critical sections quite differently. For the elastic section, Fig. 8, increasing ascent heating increases the critical load since the thermal stresses tend to move the load centroid towards the skin, thus reducing the load coupling. The decrease in critical load for descent heating is aggravated by the load centroid movement away from the skin.

For the inelastic-flexure-torsion section the critical load decreases with increasing ascent or descent gradients because of modulus reductions. Unlike the elastic sections, the free-flange stress tends to decrease with increasing gradient. This is attributed to the end load redistributions due to modulus changes. For increasing gradient to 80°F the skin flange stress shows a consistent trend. However, above 80°F the thermally induced tension stresses drive the total stress back into the elastic range and the trend is again controlled by thermal stress.

Conclusion

A general method of solution for the buckling of stiffened panels including nonlinear material behavior, thermal gradient, early skin buckling and all possible panel modes was presented. It has been demonstrated by test and analysis correlation, that by judicious selection of elements and modes, solutions can be obtained which are commensurate with engineering accuracy and the limitations on available computer resources. A simplified hand solution was presented to illustrate the mechanics of the computations. Application of the method to a variety of titanium panels demonstrated the importance of distortion and torsional modes to titanium compression panel design. Correlations with tests of these panels are within ±15%. The critical panel load is strongly dependent on thermal gradients and the resulting stresses, load redistributions and modulus changes. The method has given additional insight into the complex interdependency that these factors have on the buckling load.

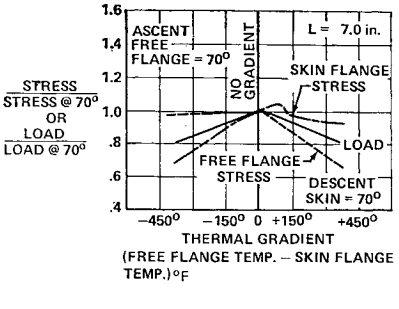

Fig. 9 Stress and load vs thermal gradient, flexure-torsion inelastic section.

References

[1] Bleich, F., "Buckling of Centrally Loaded Columns by Torsion and Flexure," *Buckling Strength of Metal Structures*, McGraw-Hill, New York, 1952, pp. 104–116.

[2] Wagner, H., "Torsion and Buckling of Open Sections," TM 807, Oct. 1936, NACA.

[3] Goodier, J. N., "Flexural-Torsional Buckling of Bars of Open Section," Bulletin No. 28, 1942, Cornell Univ. Engineering Experiment Station, Ithaca, N.Y.

[4] Argyris, J. H., "Flexure-Torsion Failure of Panels," *Aircraft Engineering*, June–July 1954, pp. 2–19.

[5] Timoshenko, S. P., "Buckling of Thin Plates," *Theory of Elastic Stability*, 2nd ed., McGraw-Hill, New York, 1961, pp. 415–417.